Mud redeposition during river incision as a factor affecting authigenic 10 Be/ 9 Be dating: Early Pleistocene large mammal fossil-bearing site Nová Vieska, eastern Danube Basin

Michal Šujan, Régis Braucher, Andrej Chyba, Martin Vlačiky, Kishan Aherwar, Barbara Rózsová, Klement Fordinál, Juraj Maglay, Alexander Nagy, Martina Moravcová, et al.

Mud redeposition during river incision as a factor affecting authigenic 10 Be/ 9 Be dating: Early Pleistocene large mammal fossil-bearing site Nová Vieska, eastern Danube Basin

Michal Šujan[1,*], Régis Braucher[2], Andrej Chyba[3], Martin Vlačiky[4], Kishan Aherwar[1], Barbara Rózsová[1], Aster Team[2]

Klement Fordinál, Juraj Maglay, Alexander Nagy?

1 – Department of Geology and Paleontology, Faculty of Natural Sciences, Comenius University in Bratislava, Ilkovičova 6, 842 15 Bratislava, Slovakia; michal.sujan@uniba.sk

2 – CNRS-IRD-Collège de France-INRA, CEREGE, Aix-Marseille Univ., 13545 Aix-en-Provence, France

3 – Institute of Chemistry, Slovak Academy of Sciences, Dúbravská cesta 9, 845 38 Bratislava, Slovakia

* – corresponding author

Abstract

This study examines the suitability of the authigenic 10Be/9Be dating method to the dating of the deposits of an incising river, taking as an example the Nová Vieska river terrace, which accumulated during the neotectonic inversion of the Danube Basin (western Slovakia). The succession was formed by a wandering river with minor preservation of proximal floodplain muds. The frequent occurrence of mud intraclasts reflects significant input of eroded material from underlying, older successions. The ages of 13 authigenic 10Be/9Be dating samples formed three groups: (1) samples from below the base of the river terrace yielded dates of ~4.13–3.70 Ma (including uncertainties); (2) muddy intraclasts from the river terrace gave an age range of ~2.79–1.96 Ma; and (3) in situ muddy layers had ages in the range of ~1.91–1.39 Ma. The large mammal fossil assemblage from channel thalweg deposits yielded a biostratigraphic age of ~3.6–2.2 Ma, matching the age of intraclasts, and thus emphasising the redeposited origin of those fossils. The relatively wide range of authigenic 10Be/9Be dating ages is interpreted as a result of the redeposition of mud from older strata on three scales: decimetre!scale intraclasts, millimetre!scale rip!up clasts mixed into the newly formed beds, and formation of two authigenic rims with different age and 10Be/9Be records around individual particles. Considering these observations, an age range of in situ layers of ~1.91–1.39 Ma is proposed as the depositional age of the river terrace, with the most probable age falling within the most recent part of this interval. The effect of redeposition is thus shown to be potentially limiting to

the application of authigenic 10Be/9Be dating to incising rivers, and stands in marked contrast to aggrading river settings, where redeposition of older sediments is limited and the degree of 10Be/9Be variability is low.

Key words: cosmogenic nuclides, authigenic beryllium, facies analysis, wandering river, redeposition, intraclasts, cryogenic deformations

1. Introduction

The authigenic $^{10}Be/^{9}Be$ dating method allows dating deposition of a clay-bearing sediment, provided that certain conditions are fulfilled (Bourlès et al., 1989; Lebatard et al., 2008; Šujan et al., 2016; Simon et al., 2020). Despite this great potential to maintain a depositional age for the most common type of sediment on the Earth (Schieber, 1998), limits of this method in continental environments are still not fully revealed. Complexity of factors possibly affecting the method rises from the different source of both isotopes employed in the system, as the radionuclide ^{10}Be being produced in the atmosphere by cosmic rays, while the stable ^{9}Be is derived by weathering of rocks. Both isotopes are mixed in a water column and incorporated into authigenic phase on the surface of sediment particles (Bourlès et al., 1989; Willenbring and von Blanckenburg, 2010; Wittmann et al., 2017; Bernhardt et al., 2020).

It has been shown that sedimentary successions accumulated in endorheic lacustrine basins, located in a craton setting with low tectonic activity and stable provenance, such as the Chad Basin in Africa, are beneficial for utilization of the method (Lebatard et al., 2008; Lebatard et al., 2010; Novello et al., 2015). The Danube Basin in more challenging conditions of an Alpine orogenic belt was proven to be suitable for dating using authigenic $^{10}Be/^{9}Be$, especially its alluvial sequence, thanks to the high accommodation to sediment supply rate (Šujan et al., 2016; Šujan et al., 2020). On the other hand, the alluvial succession in Upper Thrace Depression, Bulgaria, showed high authigenic $^{10}Be/^{9}Be$ variability preventing effective application of the

method (Schaller et al., 2015), likely due to the significant tectonic activity of the pull-apart basins in this extensional province (Burchfiel et al., 2000).

This study aims to widen the knowledge about the applicability of the authigenic $^{10}Be/^{9}Be$ dating to alluvial sediments. A hypothesis to test is the assumption that one of the major factors affecting the beryllium isotopic ratio appears to be redeposition of older sediments, when river recycles its own floodplain during incision and older mud particles are incorporated into newly formed strata. The continuous growth of authigenic rims records changing $^{10}Be/^{9}Be$ ratio in a water column (Wittmann et al., 2017), whereas the shift in isotopic ratio might be caused by different age of the authigenic rim formation, associated to the process of redeposition of older mud particles.

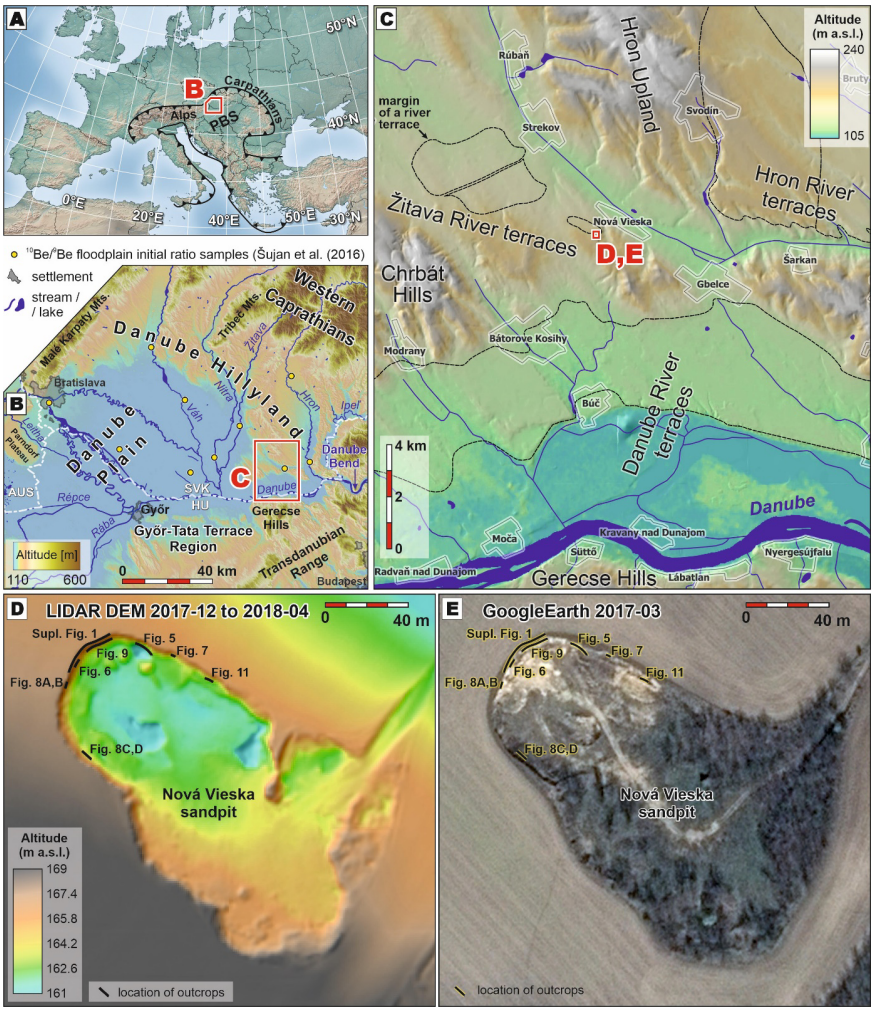

Fig. 1. Location of the study area. (A) Location of the Danube Basin within the Alpine-Carpathian orogenic belt. PBS – Pannonian Basin System (B) General topography of the Danube Basin and the present river network, with distribution of the samples used for calculation of the alluvial initial $^{10}Be/^{9}Be$ ratio in Šujan et al. (2016). (C) Topographic map of the vicinity of the Nová Vieska locality with marked margins of the river terraces of the Danube, Hron and Žitava rivers. (D) Lidar digital elevation model of the Nová Vieska sandpit showing the position of sampled outcrops. (E) GoogleEarth image of the Nová Vieska sandpit showing the position of sampled outcrops.

The Nová Vieska river terrace in the eastern Danube Basin (Slovakia) was selected for this study (Vlačiky et al., 2008; Vlačiky et al., 2017) (Fig. 1). The Early Pleistocene age of the locality was assumed based on the wealth of large mammal fossils, which were accumulated in coarse clastic channel-fill deposits. The succession was formed during inversion of the basin, when river gradually incised into its older alluvial sediments along with formation of river terrace staircases (Šujan and Rybár, 2014; Ruszkiczay-Rüdiger et al., 2018; Ruszkiczay-Rüdiger et al., 2020; Šujan et al., 2021). A detailed sedimentological analysis was performed with the goal to associate the observed authigenic $^{10}Be/^{9}Be$ variability to processes of alluvial mud redeposition in the river channel during the incision.

2. Geological setting

The Danube Basin is the northwesternmost depocenter of the Pannonian Basin System (Fig. 1A), and is surrounded by the Eastern Alps, Western Carpathians and the Transdanubian Range (Fig. 1A,B). It experienced four rifting phases during the period of ~16.0–9.5 Ma, with the last one giving rise to Lake Pannon in the region during the Late Miocene (Magyar et al., 1999; Kováč et al., 2011; Magyar et al., 2013; Sztanó et al., 2016; Šujan et al., 2021)(Fig. 2). The regression of Lake Pannon, caused by the progradation of deltaic to shelf slope depositional systems from the northwest to southeast (Magyar et al., 2013), led gradually to the dominance of alluvial deposition of the Volkovce Formation. High accommodation rate to sediment supply ratio conditions during sedimentation led to a high content of muddy floodplain facies reaching 50–80% (Šujan et al., 2020).

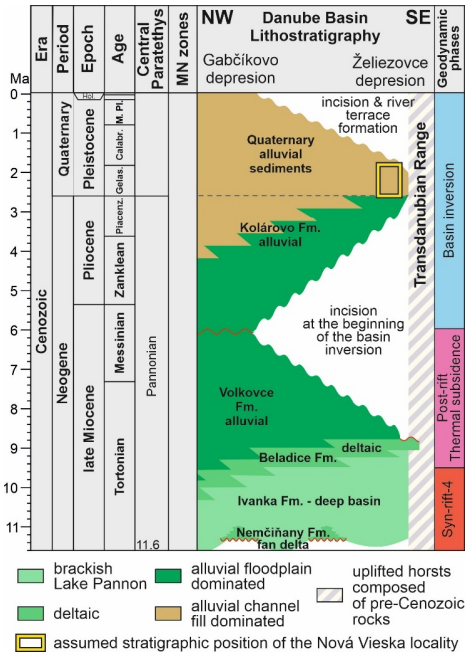

Fig. 2. Stratigraphy of the eastern Danube Basin with indication of the position of studied locality (Šujan et al., 2021). The studied succession was deposited during incision into thick underlying alluvial deposits, formed by the same rivers.

The floodplain-dominated sedimentation of the Volkovce Fm. ceased at ~6 Ma, when the basin inversion started (Tari, 1994; Vakarcs et al., 1994; Horváth, 1995; Horváth et al., 2006; Tari et al., 2020; Šujan et al., 2021). The basin inversion caused significant decrease in accommodation rates, uplift and partial denudation of the basin margins and subsidence of the central depression of the basin (Šujan et al., 2018) (Fig. 2). The syn-inversion alluvial deposition of the Kolárovo Formation gradually expanded from the central depression later on, and reached the margins of the basin at ~4–3 Ma (Ruszkiczay-Rüdiger et al., 2020; Šujan et al., 2021). The uplift of the margins overwhelmed the base-level rise after ~3 Ma, and river terraces started to be formed coevally with incision into the underlying alluvial Kolárovo Fm. and Volkovce Fm. (Šujan et al., 2021) (Fig. 2). One of the oldest sedimentary bodies deposited during this phase of the basin

evolution is the Nová Vieska river terrace, investigated in this study. Base-level fall and low accommodation conditions led to the prevailing deposition of coarse-grained channel-fill facies in the regime of a wandering river in the Nová Vieska succession (Vlačiky et al., 2008). The uplift of the area continues up to the present day, what constraints active alluvial deposition mainly to the central depression of the basin (Fig. 2C). The Nová Vieska terrace is therefore in the middle of three terrace river systems, with Hron River stepping back to the east, Žitava River to the northwest and the Danube River to the south (Fig. 1C).

The Nová Vieska sandpit is located in an altitude range of 161 to 168 m a.s.l. (Fig. 1D), ca. 60 m above the water level on the present Danube River. The river terrace succession attains relatively low thickness not exceeding ~6 m. The walls facing northeast, southeast and southwest are excavated actively mostly due to the regular paleontological campaigns (Fig. 1D,E). The river terrace deposits are accumulated above the muds and sands of the floodplain that dominated Volkovce Fm. of the Late Miocene age (Vlačiky et al., 2008; Šujan and Rybár, 2014; Šujan et al., 2020).

3. Large mammal biostratigraphy

[A REVIEW OF PUBLISHED DATA TO BE ADDED]

Fig. 3. Overview of the large mammal fossil findings from the Nová Vieska sandpit and their chronostratigraphic range.

4. Methods

4.1 Sedimentology

The detailed facies analysis of the locality was performed by Vlačiky et al. (2008), nevertheless, continuous excavations led to exposure of new sedimentary bodies, allowing to verify the previous sedimentological assumptions. Hence, the sedimentological logs and schemes of the

facies distribution on vertical outcrop walls was performed with two aims: (1) to interpret the depositional processes and asses the character of sedimentary environment, and (2) to precisely record the facies character of the strata sampled for dating, in order to understand possible variability in depositional processes that may affect the dating result. The field campaign and sampling took place during the years 2015, 2016 and 2017. The standard facies analysis of clastic sediments included description of grain size, structure, texture, geometry and size of the strata, and visualization of the gained information in logs and schemes (Stow, 2005; Miall, 2006). Paleocurrent directions of cross-strata were measured to evaluate the character of accretion of alluvial bars (Almeida et al., 2016), however, specific data are not presented due to the mainly geochronological focus of the study.

3.2 Authigenic $^{10}Be/^{9}Be$ dating

3.2.1 Principles of the method

The authigenic beryllium dating is based on the 10Be/9Be ratio measurement of stable nuclide ^{9}Be originating from chemical weathering of rocks, and of radioactive nuclide ^{10}Be produced by secondary cosmic rays in the atmosphere through spallation reaction on oxygen and nitrogen (Dunai, 2010). The ^{10}Be being very reactive gets adsorbed in aerosols and is transferred to the Earth surface in soluble form by precipitation (Raisbeck et al., 1981). ^{10}Be is removed from water column in aqueous settings and is incorporated in the authigenic phase, composed mostly of amorphous oxy-hydroxides, which cover the surface of sedimentary particles (Bourlès et al., 1989). The half-life of ^{10}Be of 1.387 ± 0.012 Ma (Chmeleff et al., 2010; Korschinek et al., 2010) offers the possibility to date the formation of the authigenic phase and hence deposition of sediments in the age range of 0.2 to 14 Ma (Ku et al., 1982; Bourlès et al., 1989; Lebatard et al., 2008), providing that the dated systems was chemically closed.

The age calculation is based on the radioactive decay of an initial concentration that follows the following equation : $N_{(t)}=N_0e^{-\lambda t}$, where $N_{(t)}$ is the authigenic $^{10}Be/^{9}Be$ ratio measured in the sample to be dated, N_0 is the initial authigenic $^{10}Be/^{9}Be$ ratio, λ is the ^{10}Be radioactive decay constant, and t is the time elapsed since deposition. This equation implies the essential need to establish the initial isotopic ratio, which depends on several factors such as the drainage basin lithology, denudation intensity, the latitude of the study area, depositional environment conditions and the proximity of the source of sediment to the place of deposition (Brown et al., 1992; Graham et al., 2001; Graly et al., 2010; Wittmann et al., 2012; Wittmann et al., 2017). Thus, the initial isotopic ratio might be established by analysis of samples taken from the same basin and with similar depositional conditions as the dated samples, which are either of the age 0–200 ka and assumed as actual, or of an independently determined age and the time elapsed is included in the calculation of the initial ratio. The analysis of a set of Holocene floodplain samples distributed across the Danube Basin (Fig. 1B) yielded a relatively low variability of authigenic $^{10}Be/^{9}Be$ values, what allowed to calculate the initial ratio for alluvial deposits used in this study with the value of $4.14 \pm 0.17 \times 10^{-9}$ (Šujan et al., 2016). Of course, the main assumption is that this ratio has remained stable through time

3.2.2 Sampling strategy and sample processing

Application of the authigenic $^{10}Be/^{9}Be$ dating to the Nová Vieska river terrace was decided as reasonable, since (1) the low thickness of the accumulation <6 m is expected to cause saturation of the *in situ* cosmogenic nuclide production in the context of the expected age of ~1.8–2.6 Ma, which would provide only a minimum exposure age, and (2) a relatively frequent presence of muddy alluvial strata within the sandy-gravelly succession, suitable for the method.

The samples for the authigenic $^{10}Be/^{9}Be$ dating were collected subsequently during the years 2015, 2016 and 2017, as new sedimentary units were exposed by continuous excavation. The sampling was focused on the muddy alluvial strata deposited either as overbank fines, or as

oxbow lake fills or muddy accretion on bars. All the mentioned types of sampled facies are denoted here as *in situ* strata and provided 8 samples. In addition to the *in situ* strata, three samples were taken from redeposited intraclasts of alluvial mud. The lithology of the sampled intraclasts was visually comparable to the *in situ* layers. The strata, from which *in situ* as well as intraclast samples originate, are considered to represent single succession of a river terrace. Two samples were taken from the thick, muddy horizon, which appeared below the base of the river terrace.

The six samples taken in 2015 (first group) were processed at CEREGE, Aix-en-Provence (France), while the seven samples taken in the following years 2016 and 2017 (second group) underwent processing in the laboratory of the Department of Geology and Paleontology, Faculty of Natural Sciences, Comenius University in Bratislava (Slovakia). The workflow applied at both laboratories followed the methodology described by Bourlès et al. (1989) and Carcaillet et al. (2004). The authigenic phase was extracted from powdered samples using a leaching solution of acetic acid, hydroxilamonium hydrochloride and demineralized water. Aliquots taken from the resulting solution were analyzed to determine the concentrations of ^{9}Be using atomic adsorption spectrometry (AAS – first group) and by inductively coupled plasma mass spectrometry (CP-MS – second group). Replicability and consistency of both approaches was tested with positive results. The following processing involved addition of 300 mg (first group) or 450 mg (second group) of the Scharlau beryllium ICP standard solution (1000 ppm) with ^{10}Be/^{9}Be ratios in the range of 6–8 × 10^{-15} (Merchel et al., 2021). Samples were evaporated and resin chemistry was applied to separate beryllium from other elements present in the authigenic phase (Merchel and Herpers, 1999). The purified samples were oxidized at 700°C for one hour in an oven, mixed with Niobium powder then transferred to copper cathodes for accelerator mass spectrometer (AMS) measurements. AMS measurements of ^{10}Be/^{9}Be isotopic ratios were done at the French national facility ASTER (CEREGE, Aix-en-Provence, France).

The AMS $^{10}Be/^{9}Be$ ratios of all samples reached values at least two orders of magnitude higher comparing to the two processing blanks and were normalized to their isotopic ratios. The calculated ages with one σ uncertainties were statisctically processed by KDX application on the Fig. 4 (Spencer et al., 2017).

3.3 Burial $^{26}Al/^{10}Be$ dating

Application of the burial $^{26}Al/^{10}Be$ dating to river sediments follows an assumption that quartz-bearing material was exposed on the Earth's surface to cosmic rays, then underwent denudation and fluvial transport, and finally was deposited and buried by aggradation of an alluvial succession. Nuclear reactions caused by interaction of quartz material with high-energy neutrons and muons included in secondary cosmic rays result in production of terrestrial cosmogenic nuclides ^{10}Be and ^{26}Al (Braucher et al., 2013; Balco, 2017). Considering long-enough surface exposure of a quartz clast, the $^{26}Al/^{10}Be$ ratio obtained at surface (denudational steady state) and is decreasing after burial due to radioactive decay with different half-lives of both radionuclides (e.g., Gosse and Phillips, 2001; Granger and Muzikar, 2001). Nevertheless, a depth of ~40 m below a rock or sediment is required for total shielding of cosmic rays, and hence post-burial production of cosmogenic nuclides may be involved into burial age calculation in the case of lower thickness of the overlying strata. The absolute concentrations of both nuclides together with their ratio could be employed also in determination of the maximum denudation rate before the burial of a sample (von Blanckenburg, 2005).

Sediment of the sandy-gravelly lithofacies SGmp was sampled in the position with thickest overburden reaching 6.6 m, providing the best available shielding for the burial dating. Nevertheless, the relatively low burial depth allows for calculation of only a minimum burial age. The sample was sieved and separated into two sub-samples, first containing quartz and quartzite pebbles (sample 6.6A) and the second one consisting sieved sandy fraction 0.25–1.00

mm (sample 6.6B). The sample composed of pebbles was crushed and sieved to the fraction 0.25–1.00 mm.

Chemical processing of the samples was performed at CEREGE, Aix-en-Provence (France). The samples underwent magnetic separation and two rounds of leaching in a solution of hexafluorosilicic and hydrochloric acid to eliminate other silicates (Merchel et al., 2019). The following sequential leaching in HF was repeated three times to dissolve the surficial parts of the grains potentially contaminated by the atmospheric ^{10}Be. An amount of ~100 µl of a (3025 ± 9) ppm of ^{9}Be in-house standard solution (Merchel et al., 2008) was added to the pure quartz, which was then totally dissolved in HF. An aliquot for ICP-OES measurements of concentrations of stable aluminium was taken after evaporation of the solution. Standard procedures of ion exchange chromatography were applied to separate Be and Al (Merchel and Herpers, 1999). Beryllium and aluminum hydroxides were oxidized and cathoded for AMS measurements, which were performed at French national facility ASTER (CEREGE, Aix-en-Provence, France).

5. Results

5.1 Facies analysis

Description of eight distinguished facies, their internal fabric, geometry and interpreted depositional processes are included in Table 1. The depositional record exhibits a prevailing coarse-grained nature, with the alternation of sandy-gravelly and sandy units. *In situ* muddy strata represent <15% of the documented succession. Lithofacies SGpm, St and Stb comprise the major volume reaching ca 60–70% proportion (Figs. 5–8). Lithofacies Sl is common, forming up to 20% locally (Fig. 5), while lithofacies Sr is rare and appears in few centimeters thin horizons or lenses (Fig. 6). All lithofacies are frequently arranged in inclined units of variable lithology 0.5 to 2.5 m thick (Figs. 5, 6, 8).

Beside the primary structures summarized in the Table 1, the locality Nová Vieska shows a wide range of penecontemporaneous deformations. Fig. 9 shows large involution structure (Vandenberghe, 2013), reaching thickness of >3 m in the lower part of the outcrop. The deformation partly preserves original structures, since rotated trough cross-bedding is observable in a number of horizons in Fig. 9E. The involution of strata caused sub-vertical orientation of the remnants of the primary bedding locally (Fig. 9F). The large involution is associated with decimeter-scale graben-like brittle collapse features, bounded by small faults, but also showing bending on the margins (Fig. 9G). The involution structure is cut by an erosional surface, while the overlying facies of Stb and St are undeformed.

Relatively common deformations comprise sand wedges reaching height of 5–20 cm (Fig. 10A). The deformation is limited from the lower part, includes bending of the surrounding strata and filling of the wedge by the overlying strata. Symmetrical rounded few centimeters to 15 cm high bending of the strata downwards with decreasing intensity of deformation towards the base is observed rarely (Fig. 10B).

Table 1. Description and interpretation of the lithofacies documented in the outcrops.

Code	Lithofacies description	Lithofacies geometry	Depositional process	Sedimentary environment	References
SGpm	coarse-grained sand with granules and mud intraclasts, ocasionally pebbles, massive to poorly-visible cross stratification, redeposited large mammal fossils	tabular and lenticular bodies with sharp base of complicated morphology and sharp upper boundary, 10–60 cm thick	rapid deposition from a wanning flow with high concentration of coarse-grained sediment	decelerating flood in a river channel	Mulder and Alexander (2001); Carling and Leclair (2019); Ghinassi and Moody (2021)
St	trough cross-stratified medium to coarse sand, occasionally with fine gravel or mud intraclasts at the base	lenticular body with sharp concave upwards base and sharp upper boundary, 10–50 cm thick	sandy bedload channelized traction current	3D dunes migrating in shallow parts of a channel and across bars	Allen (1982); Leclair and Bridge (2001); Reesink and Bridge (2011); Naqshband et al. (2017)
Stb	trough and planar cross-stratified units, foresets composed of various lithology (mud, intraclasts, fine- to coarse-grained sand, granules), strata form commonly internal angular contacts, foresets are occasionally formed by small scale trough cross-stratified sands and ripple cross-stratified sands with paleocurrent direction perpendicular to the foreset dip direction	lenticular body with sharp base of complicated morphology and sharp upper boundary, 20–60 cm thick	traction current of variable speed from ≤10 $cm \cdot s^{-1}$ to ~100 $cm \cdot s^{-1}$, flowing over an inclined surface	unit bar in a river channel, foresets formed by collapse of superimposed bedforms at the brink point (downstream accretion), or by bedforms migrating parallel to the bar surface strike (lateral accretion)	Miall (1985); Almeida et al. (2016); Reesink (2018)
Sl	medium- to coarse-grained sand with low angle inclined stratification, commonly lamination parallel to the basal acretionary surface, internal low-angle angular contacts of strata common	tabular bodies few cm thick with sharp boundaries	channelized traction current of upper plane bed flow to supercritical flow	upper plane beds to antidunes formed above bars in river channel during floods with increased flow speed	Bennett and Best (1997); Fielding (2006); Naqshband et al. (2017)
Sr	unidirectional ripples formed from medium- to fine-grained sand to silt	tabular body few cm thick with fluent boundaries or few cm thick lenticular body	shallow or slow traction current	ripples formed on a bar surface, in shallow channel or proximal overbank settings	Allen (1982); Baas (1999); Yawar and Schieber (2017)
Sm, FSm	massive medium to fine sand, containing muddy intraclasts, massive sandy mud	lenticular bodies 5-20 cm thick, with concave sharp erosional base and sharp upper boundary	rapid deposition from a wanning flow	suddenly decelerating flood in abandoned shallow channel, in an oxbow lake or in a proximal floodplain	Mulder and Alexander (2001); Baas et al. (2016), Burns et al. (2017)
Fl	planar laminated mud, beige to light grey, lamination subhorizontal or pallalel to the basal surface	continuous horizons few centimeters to 20 cm thick, with sharp lower and upper boundary	deposition from a slow traction current or from suspension	slack water deposition above a bar, in an oxbow lake or in a proximal floodplain	Aslan and Autin, (1999); Yawar and Schieber (2017)
Fm	massive mud, beige to light grey, locally lateral transition to intraclasts	continuous horizons and lenticular bodies few centimeters to 30 cm thick, with sharp lower and upper boundary	deposition from suspension of a high mud-concentrated wanning flow	decelerating flood with high content of mud, oxbow lake or proximal floodplain	Toonen et al. (2011); Baas et al. (2016)

5.2 Authigenic $^{10}Be/^{9}Be$ dating

Measured concentrations of nuclides, natural authigenic $^{10}Be/^{9}Be$ ratios and calculated ages are included in Table 2 and depicted on Fig. 4. Natural $^{10}Be/^{9}Be$ range from 5.541×10^{-10} to 20.175×10^{-10}. Ages reach values from 1.438 ± 0.048 Ma to 4.024 ± 0.111 Ma. The highest ages of 4.024 ± 0.111 Ma and 3.802 ± 0.094 Ma were yielded by the samples NV-2-4 and NV-2-5 taken from the basal muddy horizon, present below the base of the river terrace. Another group of ages is represented by the intraclast samples NV-1-4, NV-1-5 and NV-1-6, which attain 2.701 ± 0.093 Ma, 2.484 ± 0.096 Ma and 2.031 ± 0.076 Ma. The remaining seven samples originating from *in situ* layers reach ages in the range from 1.852 ± 0.060 Ma to 1.438 ± 0.048 Ma, except for the age 2.303 ± 0.093 Ma of sample NV-1-1, which appears to be an outlier. The ages of *in situ* samples are not distributed systematically regarding their vertical or lateral position.

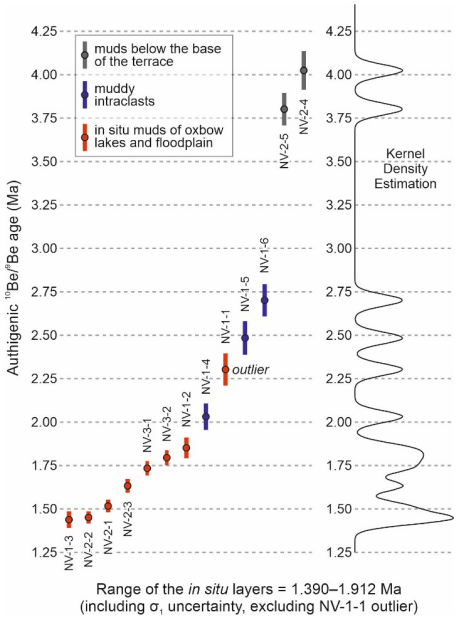

Fig. 4. Distribution of the authigenic $^{10}Be/^{9}Be$ ages depicted in ascending order of the values and Kernel Density Estimation, obtained by KDX application (Spencer et al., 2017). Depicted uncertainties are σ_1.

Table 2. Concentrations of ^{9}Be and ^{10}Be, $^{10}Be/^{9}Be$ ratios and calculated ages for the analyzed samples. Uncertainties are σ_1. Concentrations of ^{10}Be are corrected to the $^{10}Be/^{9}Be$ ratios of the two processing blanks reaching values of 7.75×10^{-15}, (sampling in 2016 and 2017) and 1.52×10^{-14} (sampling in 2015).

Commenté [RB1]: present these raw data before kdx figure

Sample ID	Year of sampling	Sample type	AMS $^{10}Be/^{9}Be$ [$\times 10^{-12}$]	AMS uncertainty $^{10}Be/^{9}Be$ [%]	^{9}Be measurement	Natural ^{9}Be [atom g $\times 10^{16}$]	^{9}Be standard deviation [%]	Natural ^{10}Be [atom g $\times 10^{7}$]	Uncertainty ^{10}Be [atom $\cdot$ g $\times 10^{7}$]	Natural $^{10}Be/^{9}Be$ [$\times 10^{-10}$]	Uncertainty $^{10}Be/^{9}Be$ [$\times 10^{-10}$]	Authigenic $^{10}Be/^{9}Be$ depositional age [Ma]
NV-1-1	2015	in situ layer	1,545	3,503	AAS	2,391	2,941	3,132	0,110	13,098	0,528	2,303 ± 0,093
NV-1-2	2015	in situ layer	3,332	2,555	AAS	4,122	0,959	6,764	0,173	16,411	0,533	1,852 ± 0,060
NV-1-3	2015	in situ layer	3,041	2,674	AAS	3,046	1,398	6,145	0,164	20,175	0,674	1,438 ± 0,048
NV-1-4	2015	intraclast	2,936	3,171	AAS	3,961	1,429	5,942	0,188	15,002	0,562	2,031 ± 0,076
NV-1-5	2015	intraclast	2,736	3,323	AAS	4,622	1,441	5,529	0,184	11,963	0,464	2,484 ± 0,096
NV-1-6	2015	intraclast	2,503	2,800	AAS	4,712	2,931	5,057	0,142	10,733	0,369	2,701 ± 0,093
NV-2-1	2016	in situ layer	3,941	1,312	ICP-MS	6,252	5,438	12,128	0,159	19,397	0,464	1,517 ± 0,036
NV-2-2	2016	in situ layer	5,001	1,392	ICP-MS	7,667	4,980	15,371	0,214	20,049	0,489	1,451 ± 0,035
NV-2-3	2016	in situ layer	3,566	1,336	ICP-MS	5,944	5,074	10,882	0,145	18,306	0,440	1,633 ± 0,039
NV-2-4	2016	basal muds	1,739	1,912	ICP-MS	9,516	3,376	5,272	0,101	5,541	0,153	4,024 ± 0,111
NV-2-5	2016	basal muds	2,183	1,435	ICP-MS	10,785	1,968	6,679	0,096	6,193	0,152	3,802 ± 0,094
NV-3-1	2017	in situ layer	3,349	1,335	ICP-MS	5,896	2,692	10,261	0,137	17,403	0,419	1,734 ± 0,042
NV-3-2	2017	in situ layer	3,368	1,332	ICP-MS	6,084	4,145	10,270	0,137	16,881	0,406	1,795 ± 0,043

5.3 Burial $^{26}Al/^{10}Be$ dating

Commenté [RB2]: do you need this part and in general the 2 burial ages?

The two sub-samples analyzed from the same sampling point yielded comparable concentrations of ^{10}Be atoms. However, they show almost two-fold difference in concentration of ^{26}Al atoms with increased content in the sample consisting of the sieved sand. If both ages are considered as minimum burial ages due to the low burial depth, the data indicate burial age of the sampled horizon of at least 1.34 ± 0.32 Ma.

Table 3. ^{10}Be and ^{26}Al isotopic concentrations, $^{26}Al/^{10}Be$ ratios paleo-denudation rates and burial age of the analyzed samples.

Sample ID	Depth [m]	Sample type	^{10}Be [at·g^{-1}]	^{26}Al [at·g^{-1}]	$^{26}Al/^{10}Be$	Denudation before burial [m·Ma^{-1}]	Burial age [Ma]
6,6A	6,60	crushed gravels	80905 ± 4184	287955 ± 67130	3.56 ± 0.85	22,07	1.34 ± 0.32
6,6B	6,60	sieved sand 0.25–1.00 mm	88890 ± 6696	488964 ± 100507	5.5 ± 1.2	31,83	0.45 ± 0.1

6. Sedimentological interpretations

6.1 Depositional processes

Lithofacies SGpm was deposited during waning of a surge-type flow with high concentration of gravelly and sandy sediment, what led to low effectivity of turbulence causing low degree of sorting and only a weak development of stratification, which is even missing locally (Mulder and Alexander, 2001; Cartigny et al., 2013; Carling and Leclair, 2019; Ghinassi and Moody, 2021) (Figs. 5E, 6C). The base of SGpm units is usually complicated and erosional, and SGpm commonly contains intraclasts of the underlying cohesive strata (Fig. 6C). Trough cross-stratified sands were deposited as 3D dunes by traction currents (Allen, 1982; Leclair and Bridge, 2001; Reesink and Bridge, 2011; Naqshband et al., 2017) (Figs. 5D, 7, 10).

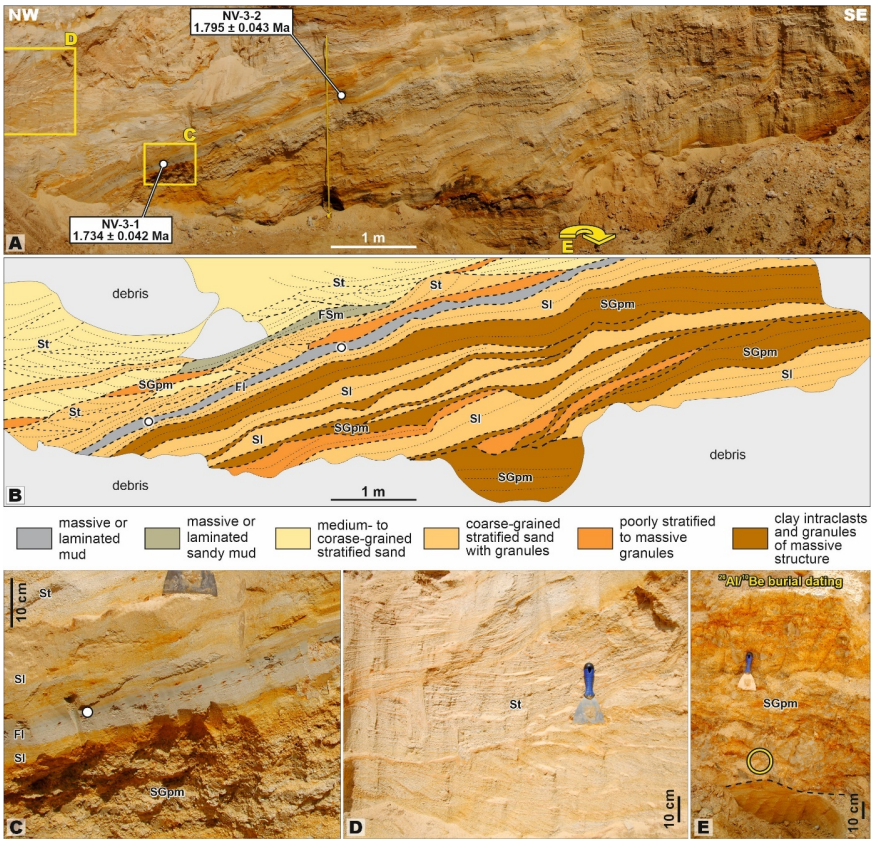

Fig. 5. Outcrop wall oriented in NW-SE direction and sampled for authigenic $^{10}Be/^{9}Be$ (white dots) and burial $^{26}Al/^{10}Be$ dating. (A,B) Inclined strata forming ca 2.5 m thick bar with variable lithology, implying changes in the current speed and sediment concentration. Orientation of trough-cross strata indicate lateral accretion origin of the bar. (C) Laminated mud strata sampled for the dating. (D) Trough cross-stratified strata. (E) Poorly sorted gravelly sand with intraclasts. For location of the outcrop, see Fig. 1D,E.

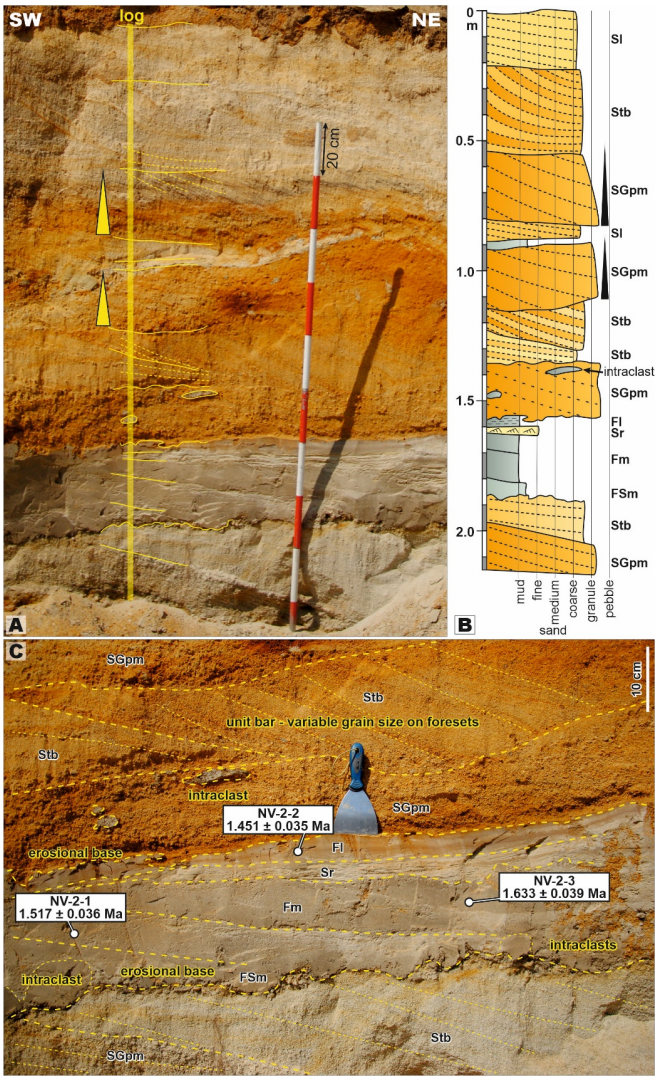

Fig. 6. Outcrop wall oriented in SW-NE direction and sampled for authigenic $^{10}Be/^{9}Be$ (white dots). Note the up to 30 cm thick, muddy horizon of a shallow oxbow lake fill and angular contacts within the unit bar of the Stb lithofacies on (C). For location of the outcrop, see Fig. 1D,E.

Facies Stb consisting of inclined strata of variable lithology from gravel to mud, and with presence of trough or ripple cross-strata within the inclined accretion units, represent fluvial

bars formed in a channel (Miall, 2006; Almeida et al., 2016; Reesink, 2018; Herbert et al., 2020). The large variability of grain size indicates significant changes in the flow speed, while internal angular contacts of the accretion units resulted from erosion preceding reactivation of a bar. According to the geometry of the accretion, it is possible to distinguish downstream-accreted unit bars (Fig. 8A,B) (Reesink, 2018), and laterally accreted point bars (Fig. 8C,D), where paleocurrent depositing superimposed dunes was oriented perpendicular to the direction of accretion (Almeida et al., 2016).

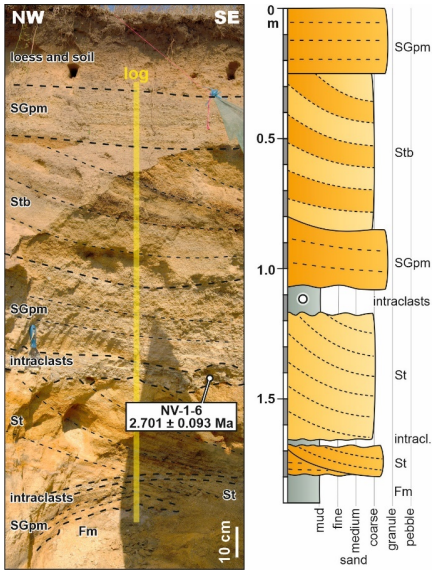

Fig. 7. Outcrop wall oriented in NW-SE direction and sampled for authigenic $^{10}Be/^{9}Be$ (white dot). The sample originate from a layer of accumulated intraclasts. For location of the outcrop, see Fig. 1D,E.

Medium- to coarse-grained sands showing subhorizontal or slightly inclined stratification or stratification parallel to an accretion surface of a bar is included in the lithofacies Sl (Figs. 5, 6, 9). It is interpreted to form upper stage plane beds or antidunes deposited by transitional or supercritical flow (Bennett and Best, 1997; Fielding, 2006; Naqshband et al., 2017). Silty, fine- to medium-grained sandy ripple cross-strata were deposited as ripple bedform by an

unidirectional traction current with low speed and/or low depth (Allen, 1982; Baas, 1999; Yawar and Schieber, 2017) (Fig. 6C). On the other hand, bodies of massive fine- to medium-grained sand (Sm) or sandy mud with intraclasts (FSm) were accumulated from a wanning surge-type flow with high concentration of sediment, possibly in an abandoned channel, in an oxbow lake or in a proximal floodplain, depending on whether the unit forms a lens in a depression or a more continuous horizon (Mulder and Alexander, 2001; Baas et al., 2016) (Fig. 6C).

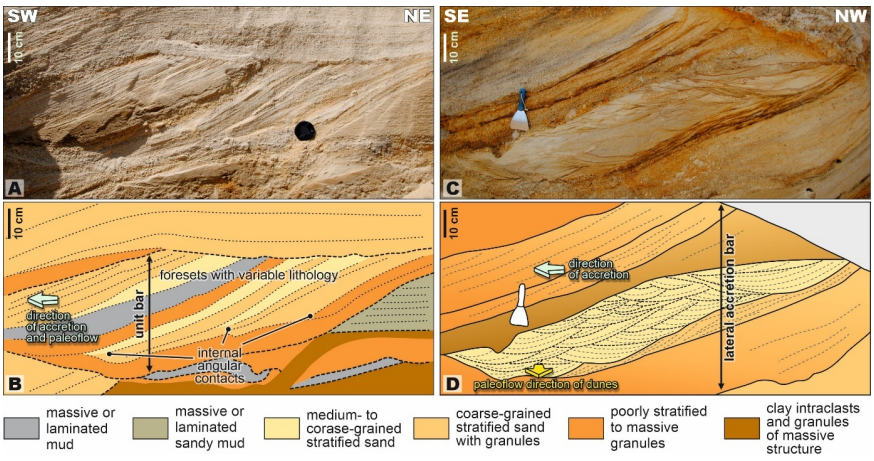

Fig. 8. Examples of a unit bar (A,B) and of lateral accretion bar (C,D). (A,B) Note the variable lithology and internal angular contacts in the unit bar, indicating variable transport capacity of a flow. (C,D) Note the perpendicular direction of bar accretion and of general paleoflow orientation indicated by trough cross-stratifications in the lateral accretion. For location of the outcrop, see Fig. 1D,E.

Planar laminated mud of the lithofacies Fl is interpreted as a deposit of slow traction current (<0.25 $m \cdot s^{-1}$) or of a suspension fallout in slack water conditions (Aslan and Autin, 1999; Yawar and Schieber, 2017) (Figs. 5C, 6, 9C,D). It was formed above a bar, in an oxbow lake or in a proximal floodplain, depending on the relation to the geometry of underlying strata. The last observed lithofacies consisting of massive mud (Fm) is frequently associated with intraclasts and its appearance indicates rapid deposition from a wanning flow with high concentration of

74 mud, likely represented by a flood decelerating in an oxbow lake or in a proximal floodplain
75 (Toonen et al., 2012; Baas et al., 2016).

76 ## 6.2 Deformations

77 The large-scale involution in Fig. 9 was formed during the deposition of the studied succession,
78 since it is overlain by undeformed strata accumulated in a river channel (Stb, St and Sl facies).
79 The deformed horizon also comprises river channel deposits, as indicated by the remnants of
80 trough cross-stratification within the deformed beds. The preservation of primary bedding and
81 the geometry of involution imply a plastic deformation by a relatively continuous process, what
82 does not favor seismic shock as a trigger. The sediment was likely under the influence of a
83 nearby stream, which deposited the overlying strata later, and hence the strata were saturated
84 with water. Accordingly, changes in rheology during freeze-thaw cycles and related loss of
85 frictional strength could be considered as the formation process of the involution (van Vliet-
86 Lanoë et al., 2004; Vandenberghe, 2013). The decimeter-scale graben-like collapses (Fig. 9G)
87 are likely associated with local extension due to frost contraction of the deformed unit. The
88 evidence for deformation of the studied strata by cryoturbation is supported by the common
89 presence of sand wedges (Fig. 10A). The wedges exhibit features of frost contraction, forming
90 of an open crack, which is than filled by the overlying sediment (Murton et al., 2000). Flame
91 structures and plastic deformation of the muds located below the base of river terrace (Fig. 11)
92 could be also explained by plastic deformation due to differential loading by freeze-thaw cycles
93 (Horváth et al., 2005; Vandenberghe, 2013). The cryogenic deformation of the basal muddy
94 horizon indicates its surface exposure during glacial. All comparable structures of cryogenic
95 deformation are commonly present in the region (Horváth et al., 2005; Ruszkiczay-Rüdiger and
96 Kern, 2016).

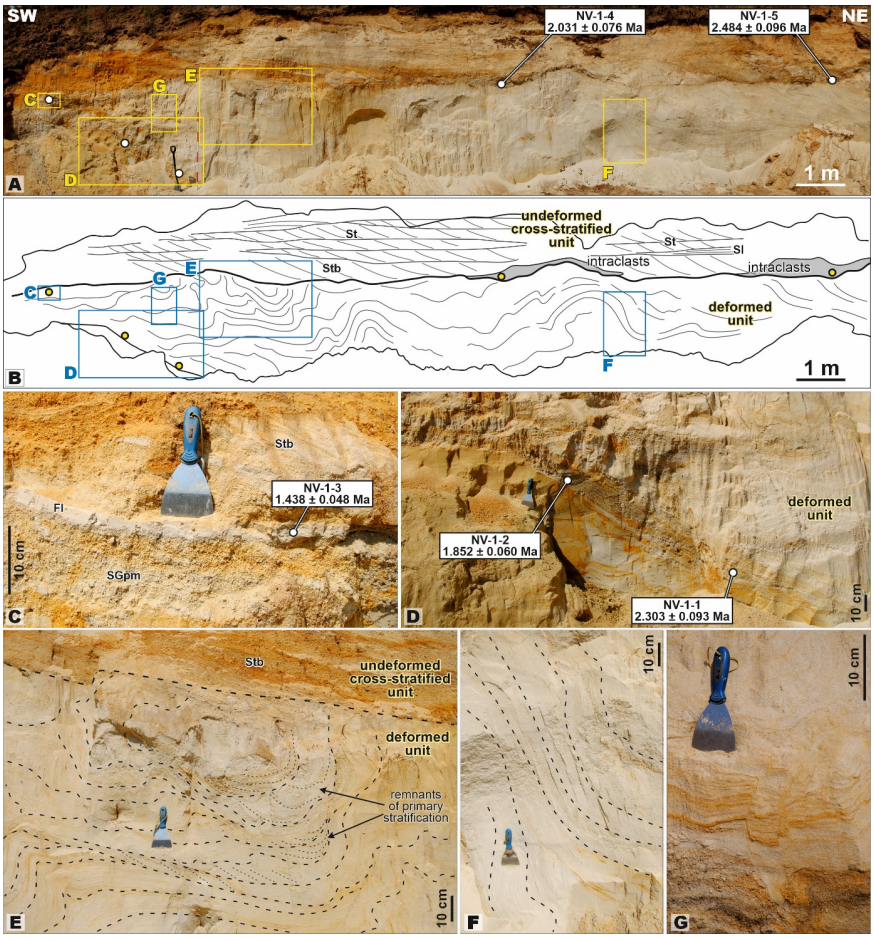

Fig. 9. Outcrop wall oriented in SW-NE direction and sampled for authigenic $^{10}Be/^{9}Be$ (white dots). (A,B) the lower unit exhibits intense deformation of the whole ca. 2.5 m thickness, while the original structures of the upper unit are preserved. Orientation of trough-cross strata indicate lateral accretion origin of the bar. (C,D) Laminated mud strata sampled for the dating. (E) Detail of the deformation with preserved remnants of the original trough cross-stratification. (F) Detail fo the deformation with almost vertically oriented strata. (G) Small-scale brittle collapse structure within the lower deformed unit. For location of the outcrop, see Fig. 1D,E.

The most rarely present deformation is symmetrical downwards bending of strata with decreasing intensity downwards (Fig. 10B). These marks are geometrically similar as foot

tracks of large mammals (Nadon et al., 2001; Fornós et al., 2002; Milán et al., 2015). However, their isolated presence in the outcrops, a relatively deep reach of the deformation and the absence of some mixing of the uppermost strata due to the impact of a foot makes this interpretation problematic. Another explanation might be deformation of the sediment by a growing tree root (do Nascimento et al., 2019). Remnants of limonitized wood are common in the SGpm facies (Vlačiky et al., 2017).

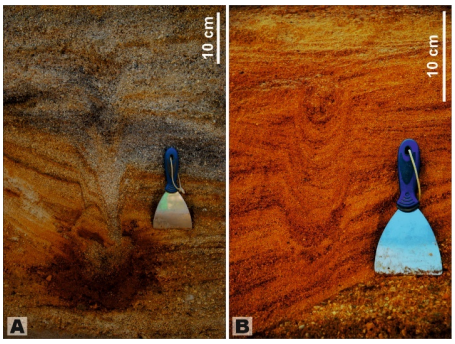

Fig. 10. Examples of deformations observable in the Nová Vieska locality. (A) Sand wedge formed by cryoturbation. (B) A mark possibly formed as a foot trace of a large mammal, or due to growth of a tree root.

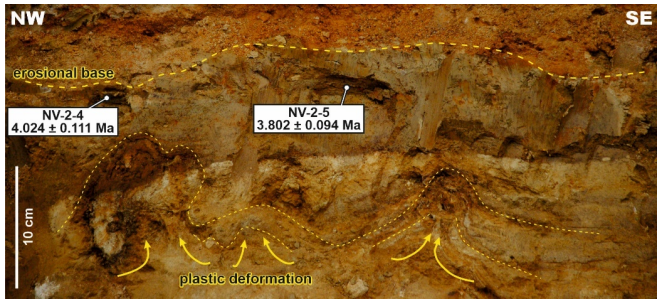

Fig. 11. Basal muds appearing below the base of the river terrace. Note the flame structure plastic deformations. For location of the outcrop, see Fig. 1D,E.

6.3 Sedimentary environment

Thickness of the bars deposited within fluvial channels vary considerably, from 0.4 m (Fig. 8) to the highest observed thickness of 2.5 m, represented by the inclined sedimentary unit in Fig. 5A,B. Thickness of a bar is generally equal to the depth of a channel, hence, the studied succession was likely accumulated by a network of channels with various depth (Bridge and Tye, 2000). Presence of both types of unit bars of downstream accretion and lateral accretion, together with low accommodation to sediment supply ratio indicated by low preservation of muddy overbank and oxbow lake facies, and indication of variable channel sizes all point to the interpretation of sedimentary environment of a wandering river (Forbes, 1983; Miall, 2006; Long and Lowey, 2011)(Fig. 12A), in agreement with the previous sedimentological research performed at the locality by Vlačiky et al. (2008). The river regime was characteristic by a deposition from perennial flow with significant proportion of surge-type flows, indicating some discharge variability was present, potentially linked to climate causes (Fielding et al., 2018; Alexander et al., 2020; Hansford et al., 2020; Herbert et al., 2020).

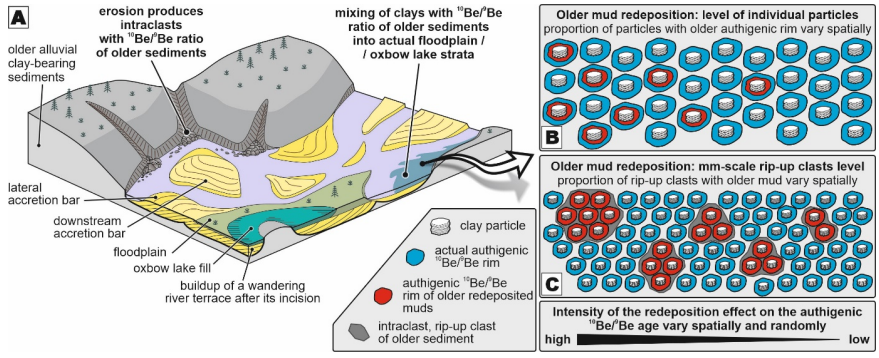

Fig. 12A. Block-diagram, showing a wandering river facies model as a sedimentological interpretation of the studied succession. The model implements incision and redeposition of underlying alluvial succession as a factor affecting the authigenic $^{10}Be/^{9}Be$ dating. Facies model modified from Miall (2006). B. Schematic hypothesis of redeposition of older mud into younger sediment by mixing at the level of individual particles. Two authigenic rims are formed around the redeposited

particles, with inner one preserving the $^{10}Be/^{9}Be$ ratio of the older bed. C. Schematic hypothesis of redeposition of older mud into younger sediment at the level of millimeter-scale intraclasts/rip-up clasts. The redeposition effect on a measured $^{10}Be/^{9}Be$ ratio of a sample is expected to vary spatially, driven by the stochastic character of random distribution of the redeposition intensity in an incising river paleoenvironment.

Considering the geomorphological position of the studied accumulation as a river terrace surrounded by hills composed of older sediments (Fig. 1C), timing of the sedimentation during the basin inversion and base-level fall recorded in the river terrace staircase formation, and abundant occurrence of clay intraclasts composed of floodplain facies, all mentioned features point to the incision, denudation of the older alluvial deposits and their redeposition as an important aspect of sedimentary environment of the Nová Vieska succession (Fig. 12).

7. Depositional age and redeposition as a factor affecting the authigenic $^{10}Be/^{9}Be$ dating

The authigenic ages show a relatively large time span, however, separating them into three groups allows determination of a narrower depositional age interval for the Nová Vieska succession. The two ages 4.024 ± 0.111 Ma and 3.802 ± 0.094 Ma obtained from the muds below the base of the river terrace imply their affinity to the Pliocene Kolárovo Formation. Thus, this formation related to the base-level rise and aggradation in the basin was at least locally preserved after the incision active after ~3 Ma, and it is not always the Volkovce Formation appearing below the river terraces in the area.

The analyzed intraclasts yielded ~0.2–1.4 Myr higher ages than the *in situ* layers, after excluding the sample NV-1-1 considered as an outlier. The depositional model shown on Fig. 12A allows to attribute this difference to a redeposition of older sediment during incision. Mixing of the older muddy sediment into younger strata on a level of individual sediment particles would result in formation of two authigenic rims around a particle, one older with $^{10}Be/^{9}Be$ ratio relevant to the redeposited sediment, and the second outer one formed at the time

of deposition with $^{10}Be/^{9}Be$ ratio of the incising river waters (Fig. 12B). Since it is not possible to separate several authigenic rims during extraction, this effect would result in apparently older authigenic $^{10}Be/^{9}Be$ age. It is assumed that the older authigenic phase was not exposed to pH<4 and therefore remains intact despite the repeated dispersion of sedimentary particles in a water column (Willenbring and von Blanckenburg, 2010). Another possible way of redeposition of older mud into younger sediment is on the level of millimeter-size rip-up clasts, scattered in the sediment with actual $^{10}Be/^{9}Be$ ratio (Fig. 12C).

The ratio of both rims forming the resulting isotopic ratio of an analyzed sample should scale to how strong is the input of older redeposited mud to a specific bed, regardless of whether it is achieved at the level of individual particles or rip-up clasts. The input of mixed older mud will vary randomly across a sedimentary environment, especially in such topographically differentiated environment as a wandering river with channels of various depth and hierarchy, and with flows of wide scale of speed, turbulence, and transport capacity. Hence, this effect should widen the range of authigenic $^{10}Be/^{9}Be$ ratios and ages within a single succession, as has been observed in the studied set of samples.

Erosion of muddy strata, production of rip-up clasts and mixing of mud by traction currents was observed in flume experiments (Schieber et al., 2010; Noack et al., 2015; Van Rijn, 2020). Even if formed from unconsolidated and non-lithified mud, the intraclasts might be prone to be transported on considerable distances (Schieber, 2016). The muddy rip-up clasts attain sub-millimeter to centimeter scale, and their presence in a bed might not be straightforward to recognize visually in the field. Processes of mud redeposition as rip-up intraclasts or a mixture are a common feature observed in fluvial environment (Müller et al., 2004; Li et al., 2017; Perkey et al., 2020; Li et al., 2021). Flows with high erosion potential took place during the deposition of the studied succession (Fig. 12A).

194 The described effect of mixing of mud with preserved older authigenic $^{10}Be/^{9}Be$ signal is
195 considered as a reasonable hypothesis for explanation of the wide range of authigenic $^{10}Be/^{9}Be$
196 ages of the *in situ* layers, which mostly do not overlap within σ_1 uncertainties. The analytical
197 uncertainties therefore can't mirror the paleoenvironmental variability caused by the
198 redeposition and mixing. Thus, it is assumed that the most robust approach in determination of
199 the depositional age of the outcrop is to use the full range of the *in situ* layers ages within error
200 bars, what yields 1.390–1.912 Ma. Since the burial $^{26}Al/^{10}Be$ dating provided only minimum
201 burial ages, it agrees with the mentioned age interval and does not allow to constrain it more
202 specifically.

203 The established depositional age is not in agreement with the age range ~2.58–1.85 Ma
204 indicated by the biostratigraphy of large mammal fossils from the succession. Nevertheless, all
205 fossils are present as clasts in the channel-fill facies, and hence were redeposited. The dated
206 intraclasts do exhibit ages fitting to the mammal biostratigraphic age range, pointing to the
207 possibility of the same source of material during redeposition.

208 The hypothesis of redeposition of older sediment as a factor affecting the authigenic $^{10}Be/^{9}Be$
209 dating needs to be further verified. A validation of the hypothesis by petrographic or
210 geochemical proxies remains problematic, as the floodplain muddy facies of the redeposited
211 Volkovce and Kolárovo fms. as well as the Quaternary sediments were deposited by
212 comparable processes and with similar provenance (Šujan et al., 2018; Šujan et al., 2020). An
213 open question remains, whether would different climatic conditions allow to trace the described
214 effect in the muddy layers. Mixing of older mud as a cause of apparently older ages of the
215 $^{10}Be/^{9}Be$ dating was documented by microfossils redeposition in the turbiditic succession
216 deposited on the basin floor of Lake Pannon in the Danube Basin (Šujan et al., 2016), however,
217 this approach is not suitable for terrestrial facies.

Extensive occurrence of cryogenic deformations and their burial point to sedimentation during glacials (Vandenberghe, 2013). Evolution of mean annual temperatures (MAT) in the period of ~2.58–1.80 Ma in the Central Europe (Kahlke et al., 2011; Kovács et al., 2015; Martinetto et al., 2015; Teodoridis et al., 2017) show values not cool enough to produce the observed deformations (Ruszkiczay-Rüdiger and Kern, 2016). Glaciation in Europe was suggested only after 1.8 Ma, and its more significant extension in the Alps and Carpathians even after 1.2–0.9 Ma (Muttoni et al., 2003; Van Husen, 2004; Gibbard and Lewin, 2009; Knudsen et al., 2020). Hence, the extensive presence of cryogenic deformations in the Nová Vieska succession favors the age range of 1.390–1.912 Ma established in this study by the authigenic $^{10}Be/^{9}Be$ dating.

8. Conclusions

This study aimed to investigate suitability of incising river deposits formed under low accommodation and high sediment supply conditions for dating using the authigenic $^{10}Be/^{9}Be$ method. The Nová Vieska river terrace succession, located in the eastern Danube Basin, comprises facies of a wandering river, composed of downstream-accreted unit bars and lateral accretion bars. Facies analysis implied a high variability of flow speed, turbulence and sediment concentration, which resulted in a wide range of lithologies from gravelly sands to *in situ* muddy strata of floodplain and oxbow lake deposits forming minor part of the succession. Redeposition of mud from older eroded strata during incision of the river, related to the ongoing inversion of the basin, was an important feature of the sedimentary environment, as is evidenced by the widespread occurrence of mud intraclasts.

The authigenic $^{10}Be/^{9}Be$ dating yielded ages divided into three groups of samples: (1) two ages of 4.024 ± 0.111 Ma and 3.802 ± 0.094 Ma from the strata below the base of the river terrace; (2) three ages of 2.701 ± 0.093 Ma, 2.484 ± 0.096 Ma and 2.031 ± 0.076 Ma obtained from intraclasts of the redeposited mud; and (3) six ages in the range of 1.852 ± 0.060 Ma to 1.438 ± 0.048 Ma yielded by analysis of in situ muddy strata, with one outlier reaching an age of

2.303 ± 0.093 Ma. Burial $^{26}Al/^{10}Be$ dating of two samples provided minimum burial ages of 1.34 ± 0.32 Ma and 0.45 ± 0.10 Ma.

The pattern of the authigenic $^{10}Be/^{9}Be$ ages distribution is interpreted to be a result of redeposition of older mud derived from the incised substrate, which consists dominantly of muddy alluvial sediments. The hypothesis of redeposition as a factor affecting the authigenic $^{10}Be/^{9}Be$ dating is proposed in three scales: (1) redeposition of decimeter-scale intraclasts with preserved original age of the older substrate, (2) redeposition of millimeter-scale rip-up clasts preserving $^{10}Be/^{9}Be$ ratio of the older substrate, which are mixed into younger strata with random proportion, and (3) redeposition at the scale of individual particles, leading to formation of two authigenic rims, the inner one preserving the older $^{10}Be/^{9}Be$ ratio, and the outer one representing the actual $^{10}Be/^{9}Be$ ratio during deposition. The proportion of particles with preserved older authigenic $^{10}Be/^{9}Be$ rim would also vary randomly across the depositional environment. The stochastic spatial variation of the admixture of older mud particles or rip-up clasts is considered to be the reason of the wide range of the ages obtained from *in situ* muddy layers. Taking into account all mentioned assumptions, the full range of the authigenic $^{10}Be/^{9}Be$ ages yielded by the *in situ* mud samples reaching 1.390–1.912 Ma (within uncertainties) is proposed as the age of deposition of the studied succession.

The established age range differs from the interval ~2.58–1.85 Ma provided by the large mammal biostratigraphy, however, these fossils are accumulated as clasts and likely underwent redeposition from the same source as the similarly aged intraclasts. Extensive occurrence of cryogenic deformations also favors the age range provided by the authigenic $^{10}Be/^{9}Be$ dating, since the climatic conditions needed to attain such deformations appeared in Central Europe only at this later time.

The hypothesis of mud redeposition during incision of a river as an effect affecting the authigenic $^{10}Be/^{9}Be$ dating needs further investigation and verification. This study emphasized

the potential influence of this effect on the dating method application in continental environments, which should be considered in future studies.

Acknowledgement

The study was supported by the Slovak Research and Development Agency (APVV) under contract Nos. APVV-16-0121 and APVV-20-0120. ASTER AMS national facility (CEREGE, Aix-en-Provence) is supported by the INSU/CNRS, the ANR through the "Projets thématiques d'excellence" program for the "Equipements d'excellence" ASTER-CEREGE action and IRD. Zsófia Ruszkiczay-Rüdiger is thanked for her kind advice during interpretation of cryogenic deformations and dating results.

References

Alexander, J., Herbert, C.M., Fielding, C.R., Amos, K.J., 2020. Controls on channel deposits of highly variable rivers: Comparing hydrology and event deposits in the Burdekin River, Australia. Sedimentology 67, 2721-2746.

Allen, J.R.L., 1982. Sedimentary Structures: Their Character and Physical Basis. Elsevier, Amsterdam.

Almeida, R.P., Freitas, B.T., Turra, B.B., Figueiredo, F.T., Marconato, A., Janikian, L., 2016. Reconstructing fluvial bar surfaces from compound cross-strata and the interpretation of bar accretion direction in large river deposits. Sedimentology 63, 609-628.

Aslan, A., Autin, W.J., 1999. Evolution of the Holocene Mississippi River floodplain, Ferriday, Louisiana: Insights on the origin of fine-grained floodplains. Journal of Sedimentary Research 69, 800-815.

Baas, J.H., 1999. An empirical model for the development and equilibrium morphology of current ripples in fine sand. Sedimentology 46, 123-138.

Baas, J.H., Best, J.L., Peakall, J., 2016. Predicting bedforms and primary current stratification in cohesive mixtures of mud and sand. Journal of the Geological Society 173, 12-45.

Balco, G., 2017. Production rate calculations for cosmic-ray-muon-produced 10Be and 26Al benchmarked against geological calibration data. Quaternary Geochronology 39, 150-173.

Bennett, S., Best, J., 1997. Bed-load motion at high shear stress: Dune washout and plane-bed flow. Journal of Hydraulic Engineering 123, 375-377.

Bernhardt, A., Oelze, M., Bouchez, J., von Blanckenburg, F., Mohtadi, M., Christl, M., Wittmann, H., 2020. 10Be/9Be Ratios Reveal Marine Authigenic Clay Formation. Geophysical Research Letters 47.

Bourlès, D., Raisbeck, G.M., Yiou, F., 1989. 10Be and 9Be in marine sediments and their potential for dating. Geochimica et Cosmochimica Acta 53, 443-452.

Braucher, R., Bourlès, D., Merchel, S., Vidal Romani, J., Fernadez-Mosquera, D., Marti, K., Léanni, L., Chauvet, F., Arnold, M., Aumaître, G., Keddadouche, K., 2013. Determination of muon attenuation lengths in depth profiles from in situ produced

cosmogenic nuclides. Nuclear Instruments and Methods in Physics Research Section B: Beam Interactions with Materials and Atoms 294, 484-490.
Bridge, J.S., Tye, R.S., 2000. Interpreting the dimensions of ancient fluvial channel bars, channels, and channel belts from wireline-logs and cores. Aapg Bulletin 84, 1205-1228.
Brown, E.T., Edmond, J.M., Raisbeck, G.M., Bourlès, D.L., Yiou, F., Measures, C.I., 1992. Beryllium isotope geochemistry in tropical river basins. Geochimica et Cosmochimica Acta 56, 1607-1624.
Burchfiel, B., Nakov, R., Tzankov, T., Royden, L., Bozkurt, E., Winchester, J., Piper, J., 2000. Tectonics and Magmatism in Turkey and the Surrounding Area. Geological Society of London Special Publication 173, 325-352.
Carcaillet, J., Bourlès, D.L., Thouveny, N., Arnold, M., 2004. A high resolution authigenic 10Be/9Be record of geomagnetic moment variations over the last 300 ka from sedimentary cores of the Portuguese margin. Earth and Planetary Science Letters 219, 397-412.
Carling, P.A., Leclair, S.F., 2019. Alluvial stratification styles in a large, flash-flood influenced dryland river: The Luni River, Thar Desert, north-west India. Sedimentology 66, 102-128.
Cartigny, M.J.B., Eggenhuisen, J.T., Hansen, E.W.M., Postma, G., 2013. Concentration-dependent flow stratification in experimental high-density turbidity currents and their relevance to turbidite facies models. Journal of Sedimentary Research 83, 1046-1064.
do Nascimento, D.L., Batezelli, A., Ladeira, F.S.B., 2019. The paleoecological and paleoenvironmental importance of root traces: Plant distribution and topographic significance of root patterns in Upper Cretaceous paleosols. CATENA 172, 789-806.
Dunai, T., 2010. Cosmogenic Nuclides. Principles, Concepts and Applications in the Earth Surface Sciences. Cambridge University Press.
Fielding, C.R., 2006. Upper flow regime sheets, lenses and scour fills: Extending the range of architectural elements for fluvial sediment bodies. Sedimentary Geology 190, 227-240.
Fielding, C.R., Alexander, J., Allen, J.P., 2018. The role of discharge variability in the formation and preservation of alluvial sediment bodies. Sedimentary Geology 365, 1-20.
Forbes, D., 1983. Morphology and sedimentology of a sinuous gravel-bed channel system: lower Babbage River, Yukon coastal plain, Canada, Modern and ancient fluvial systems. Inter. Assoc. Sedim. Spec. Publ., 6, pp. 195-206.
Fornós, J.J., Bromley, R.G., Clemmensen, L.B., Rodríguez-Perea, A., 2002. Tracks and trackways of Myotragus balearicus Bate (Artiodactyla, Caprinae) in Pleistocene aeolianites from Mallorca (Balearic Islands, Western Mediterranean). Palaeogeography, Palaeoclimatology, Palaeoecology 180, 277-313.
Ghinassi, M., Moody, J., 2021. Reconstruction of an extreme flood hydrograph and morphodynamics of a meander bend in a high-peak discharge variability river (Powder River, USA). Sedimentology 68, 3549-3576.
Gibbard, P.L., Lewin, J., 2009. River incision and terrace formation in the Late Cenozoic of Europe. Tectonophysics 474, 41-55.
Gosse, J.C., Phillips, F.M., 2001. Terrestrial in situ cosmogenic nuclides: theory and application. Quaternary Science Reviews 20, 1475-1560.
Graham, I.J., Ditchburn, R.G., Whitehead, N.E., 2001. Be isotope analysis of a 0–500 ka loess–paleosol sequence from Rangitatau East, New Zealand. Quaternary International 76–77, 29-42.
Graly, J.A., Bierman, P.R., Reusser, L.J., Pavich, M.J., 2010. Meteoric 10Be in soil profiles: a global meta-analysis. Geochimica et Cosmochimica Acta 74, 6814-6829.

354 Granger, D.E., Muzikar, P.F., 2001. Dating sediment burial with in situ-produced cosmogenic
355 nuclides: theory, techniques, and limitations. Earth and Planetary Science Letters 188,
356 269-281.
357 Hansford, M.R., Plink-Björklund, P., Jones, E.R., 2020. Global quantitative analyses of river
358 discharge variability and hydrograph shape with respect to climate types. Earth-Science
359 Reviews 200, 102977.
360 Herbert, C.M., Alexander, J., Amos, K.J., Fielding, C.R., 2020. Unit bar architecture in a
361 highly-variable fluvial discharge regime: Examples from the Burdekin River, Australia.
362 Sedimentology 67, 576-605.
363 Horváth, F., 1995. Phases of compression during the evolution of the Pannonian Basin and its
364 bearing on hydrocarbon exploration. Marine and Petroleum Geology 12, 837-844.
365 Horváth, F., Bada, G., Szafián, P., Tari, G., Ádám, A., Cloetingh, S., 2006. Formation and
366 deformation of the Pannonian Basin: Constraints from observational data, Geological
367 Society Memoir, pp. 191-206.
368 Horváth, Z., Michéli, E., Mindszenty, A., Berényi-Üveges, J., 2005. Soft-sediment deformation
369 structures in Late Miocene–Pleistocene sediments on the pediment of the Mátra Hills
370 (Visonta, Atkár, Verseg): Cryoturbation, load structures or seismites? Tectonophysics
371 410, 81-95.
372 Chmeleff, J., von Blanckenburg, F., Kossert, K., Jakob, D., 2010. Determination of the 10Be
373 half-life by multicollector ICP-MS and liquid scintillation counting. Nuclear Instruments
374 and Methods in Physics Research, Section B: Beam Interactions with Materials and
375 Atoms 268, 192-199.
376 Kahlke, R.-D., García, N., Kostopoulos, D.S., Lacombat, F., Lister, A.M., Mazza, P.P.A.,
377 Spassov, N., Titov, V.V., 2011. Western Palaearctic palaeoenvironmental conditions
378 during the Early and early Middle Pleistocene inferred from large mammal communities,
379 and implications for hominin dispersal in Europe. Quaternary Science Reviews 30, 1368-
380 1395.
381 Knudsen, M.F., Nørgaard, J., Grischott, R., Kober, F., Egholm, D.L., Hansen, T.M., Jansen,
382 J.D., 2020. New cosmogenic nuclide burial-dating model indicates onset of major
383 glaciations in the Alps during Middle Pleistocene Transition. Earth and Planetary Science
384 Letters 549.
385 Korschinek, G., Bergmaier, A., Faestermann, T., Gerstmann, U.C., Knie, K., Rugel, G.,
386 Wallner, A., Dillmann, I., Dollinger, G., von Gostomski, C.L., Kossert, K., Maiti, M.,
387 Poutivtsev, M., Remmert, A., 2010. A new value for the half-life of Be-10 by Heavy-Ion
388 Elastic Recoil Detection and liquid scintillation counting. Nuclear Instruments &
389 Methods in Physics Research Section B-Beam Interactions with Materials and Atoms
390 268, 187-191.
391 Kovács, J., Szabó, P., Kocsis, L., Vennemann, T., Sabol, M., Gasparik, M., Virág, A., 2015.
392 Pliocene and Early Pleistocene paleoenvironmental conditions in the Pannonian Basin
393 (Hungary, Slovakia): Stable isotope analyses of fossil proboscidean and perissodactyl
394 teeth. Palaeogeography, Palaeoclimatology, Palaeoecology 440, 455-466.
395 Kováč, M., Synak, R., Fordinál, K., Joniak, P., Tóth, C., Vojtko, R., Nagy, A., Baráth, I.,
396 Maglay, J., Minár, J., 2011. Late Miocene and Pliocene history of the Danube Basin:
397 Inferred from development of depositional systems and timing of sedimentary facies
398 changes. Geologica Carpathica 62, 519-534.
399 Ku, T.L., Kusakabe, M., Nelson, D.E., Southon, J.R., Korteling, R.G., Vogel, J., Nokikow, I.,
400 1982. Constancy of oceanic deposition of 10Be as recorded in ferromanganese crusts.
401 Nature 299, 240-242.
402 Lebatard, A.-E., Bourlès, D.L., Braucher, R., Arnold, M., Duringer, P., Jolivet, M., Moussa, A.,
403 Deschamps, P., Roquin, C., Carcaillet, J., Schuster, M., Lihoreau, F., Likius, A.,

Mackaye, H.T., Vignaud, P., Brunet, M., 2010. Application of the authigenic 10Be/9Be dating method to continental sediments: Reconstruction of the Mio-Pleistocene sedimentary sequence in the early hominid fossiliferous areas of the northern Chad Basin. Earth and Planetary Science Letters 297, 57-70.

Lebatard, A.E., Bourlès, D.L., Duringer, P., Jolivet, M., Braucher, R., Carcaillet, J., Schuster, M., Arnaud, N., Monié, P., Lihoreau, F., Likius, A., Mackaye, H.T., Vignaud, P., Brunet, M., 2008. Cosmogenic nuclide dating of Sahelanthropus tchadensis and Australopithecus bahrelghazali: Mio-Pliocene hominids from Chad. Proceedings of the National Academy of Sciences of the United States of America 105, 3226-3231.

Leclair, S.F., Bridge, J.S., 2001. Quantitative interpretation of sedimentary structures formed by river dunes. Journal of Sedimentary Research 71, 713-716.

Li, S., Li, S., Shan, X., Gong, C., Yu, X., 2017. Classification, formation, and transport mechanisms of mud clasts. International Geology Review 59, 1609-1620.

Li, Z., Schieber, J., Pedersen, P.K., 2021. On the origin and significance of composite particles in mudstones: Examples from the Cenomanian Dunvegan Formation. Sedimentology 68, 737-754.

Long, D.G.F., Lowey, G.W., 2011. Wandering gravel-bed rivers and high-constructive stable channel sandy fluvial systems in the Ross River area, Yukon Territory, Canada. Geoscience Frontiers 2, 277-288.

Magyar, I., Geary, D.H., Müller, P., 1999. Paleogeographic evolution of the Late Miocene Lake Pannon in Central Europe. Palaeogeography, Palaeoclimatology, Palaeoecology 147, 151-167.

Magyar, I., Radivojevic, D., Sztano, O., Synak, R., Ujszaszi, K., Pocsik, M., 2013. Progradation of the paleo-Danube shelf margin across the Pannonian Basin during the Late Miocene and Early Pliocene. Global and Planetary Change 103, 168-173.

Martinetto, E., Monegato, G., Irace, A., Vaiani, S.C., Vassio, E., 2015. Pliocene and Early Pleistocene carpological records of terrestrial plants from the southern border of the Po Plain (northern Italy). Review of Palaeobotany and Palynology 218, 148-166.

Merchel, S., Arnold, M., Aumaître, G., Benedetti, L., Bourlès, D.L., Braucher, R., Alfimov, V., Freeman, S.P.H.T., Steier, P., Wallner, A., 2008. Towards more precise 10Be and 36Cl data from measurements at the 10−14 level: Influence of sample preparation. Nuclear Instruments and Methods in Physics Research Section B: Beam Interactions with Materials and Atoms 266, 4921-4926.

Merchel, S., Braucher, R., Lachner, J., Rugel, G., 2021. Which is the best 9Be carrier for 10Be/9Be accelerator mass spectrometry? MethodsX 8.

Merchel, S., Gärtner, A., Beutner, S., Bookhagen, B., Chabilan, A., 2019. Attempts to understand potential deficiencies in chemical procedures for AMS: Cleaning and dissolving quartz for 10Be and 26Al analysis. Nuclear Instruments and Methods in Physics Research, Section B: Beam Interactions with Materials and Atoms 455, 293-299.

Merchel, S., Herpers, U., 1999. An Update on Radiochemical Separation Techniques for the Determination of Long-Lived Radionuclides via Accelerator Mass Spectrometry. Radiochimica Acta 84, 215-220.

Miall, A.D., 2006. The geology of fluvial deposits: Sedimentary facies, basin analysis, and petroleum geology, 3rd edition ed. Springier, Berlin.

Milán, J., Theodorou, G., Loope, D.B., Panayides, I., Clemmensen, L.B., Gkioni, M., 2015. Vertebrate tracks in late pleistocene-early holocene (?) carbonate aeolianites, paphos, cyprus. Annales Societatis Geologorum Poloniae 85, 507-514.

Mulder, T., Alexander, J., 2001. The physical character of subaqueous sedimentary density flow and their deposits. Sedimentology 48, 269-299.

Müller, R., Nystuen, J.P., Wright, V.P., 2004. Pedogenic mud aggregates and paleosol development in ancient dryland river systems: Criteria for interpreting alluvial mudrock origin and floodplain dynamics. Journal of Sedimentary Research 74, 537-551.
Murton, J.B., Worsley, P., Gozdzik, J., 2000. Sand veins and wedges in cold aeolian environments. Quaternary Science Reviews 19, 899-922.
Muttoni, G., Carcano, C., Garzanti, E., Ghielmi, M., Piccin, A., Pini, R., Rogledi, S., Sciunnach, D., 2003. Onset of major Pleistocene glaciations in the Alps. Geology 31, 989-992.
Nadon, G., Tanke, D., Carpenter, K., 2001. The impact of sedimentology on vertebrate track studies. Mesozoic vertebrate life, 395-407.
Naqshband, S., Hoitink, A.J.F., McElroy, B., Hurther, D., Hulscher, S.J.M.H., 2017. A Sharp View on River Dune Transition to Upper Stage Plane Bed. Geophysical Research Letters 44, 11,437-411,444.
Noack, M., Gerbersdorf, S.U., Hillebrand, G., Wieprecht, S., 2015. Combining Field and Laboratory Measurements to Determine the Erosion Risk of Cohesive Sediments Best. Water 7, 5061-5077.
Novello, A., Lebatard, A.E., Moussa, A., Barboni, D., Sylvestre, F., Bourlès, D.L., Paillès, C., Buchet, G., Decarreau, A., Duringer, P., Ghienne, J.F., Maley, J., Mazur, J.C., Roquin, C., Schuster, M., Vignaud, P., 2015. Diatom, phytolith, and pollen records from a 10 Be/ 9 Be dated lacustrine succession in the chad basin: Insight on the miocene-pliocene paleoenvironmental changes in Central Africa. Palaeogeography, Palaeoclimatology, Palaeoecology 430, 85-103.
Perkey, D.W., Smith, S.J., Fall, K.A., Massey, G.M., Friedrichs, C.T., Hicks, E.M., 2020. Impacts of Muddy Bed Aggregates on Sediment Transport and Management in the Tidal James River, VA. Journal of Waterway, Port, Coastal, and Ocean Engineering 146, 04020028.
Raisbeck, G.M., Yiou, F., Fruneau, M., Loiseaux, J.M., Lievin, M., Ravel, J.C., 1981. Cosmogenic 10Be/7Be as a probe of atmospheric transport processes. Geophysical Research Letters 8, 1015-1018.
Reesink, A.J.H., 2018. Interpretation of cross strata formed by unit bars, In: Ghinassi, M., Colombera, L., Mountney, N.P., Reesink, A.J.H. (Eds.), Fluvial Meanders and Their Sedimentary Products in the Rock Record. International Association of Sedimentologists Special Publication, Wiley-Blackwell, Oxford, pp. 173-200.
Reesink, A.J.H., Bridge, J.S., 2011. Evidence of bedform superimposition and flow unsteadiness in unit-bar deposits, South Saskatchewan river, Canada. Journal of Sedimentary Research 81, 814-840.
Ruszkiczay-Rüdiger, Z., Balázs, A., Csillag, G., Drijkoningen, G., Fodor, L., 2020. Uplift of the Transdanubian Range, Pannonian Basin: How fast and why? Global and Planetary Change 192.
Ruszkiczay-Rüdiger, Z., Csillag, G., Fodor, L., Braucher, R., Novothny, Á., Thamó-Bozsó, E., Virág, A., Pazonyi, P., Timár, G., 2018. Integration of new and revised chronological data to constrain the terrace evolution of the Danube River (Gerecse Hills, Pannonian Basin). Quaternary Geochronology 48, 148-170.
Ruszkiczay-Rüdiger, Z., Kern, Z., 2016. Permafrost or seasonal frost? A review of paleoclimate proxies of the last glacial cycle in the East Central European lowlands. Quaternary International 415, 241-252.
Schaller, M., Lachner, J., Christl, M., Maden, C., Spassov, N., Ilg, A., Böhme, M., 2015. Authigenic Be as a tool to date river terrace sediments? – An example from a Late Miocene hominid locality in Bulgaria. Quaternary Geochronology 29, 6-15.
Schieber, J., 1998. Shales and Mudstones, In: Schieber, J., Zimmerle, W., Sethi, P.S. (Eds.), I. Basin Studies, Sedimentology and Paleontology. Schweizerbart, Stuttgart, pp. 131-146.

503 Schieber, J., 2016. Mud re-distribution in epicontinental basins - Exploring likely processes.
504 Marine and Petroleum Geology 71, 119-133.
505 Schieber, J., Southard, J.B., Schimmelmann, A., 2010. Lenticular shale fabrics resulting from
506 intermitent erosion of water-rich muds - Interpreting the rock record in the light of recent
507 flume experiments. Journal of Sedimentary Research 80, 119-128.
508 Simon, Q., Ledru, M.P., Sawakuchi, A.O., Favier, C., Mineli, T.D., Grohmann, C.H., Guedes,
509 M., Bard, E., Thouveny, N., Garcia, M., Tachikawa, K., Rodríguez-Zorro, P.A., 2020.
510 Chronostratigraphy of a 1.5±0.1 Ma composite sedimentary record from Colônia basin
511 (SE Brazil): Bayesian modeling based on paleomagnetic, authigenic 10Be/9Be,
512 radiocarbon and luminescence dating. Quaternary Geochronology 58.
513 Spencer, C.J., Yakymchuk, C., Ghaznavi, M., 2017. Visualising data distributions with kernel
514 density estimation and reduced chi-squared statistic. Geoscience Frontiers 8, 1247-1252.
515 Stow, D.A., 2005. Sedimentary Rocks in the Field. A Colour Guide. Manson Publishing,
516 London.
517 Sztanó, O., Kováč, M., Magyar, I., Šujan, M., Fodor, L., Uhrin, A., Rybár, S., Csillag, G.,
518 Tokés, L., 2016. Late Miocene sedimentary record of the Danube/Kisalföld Basin:
519 Interregional correlation of depositional systems, stratigraphy and structural evolution.
520 Geologica Carpathica 67, 525-542.
521 Šujan, M., Braucher, R., Kováč, M., Bourlès, D.L., Rybár, S., Guillou, V., Hudáčková, N.,
522 2016. Application of the authigenic 10Be/9Be dating method to Late Miocene–Pliocene
523 sequences in the northern Danube Basin (Pannonian Basin System): Confirmation of
524 heterochronous evolution of sedimentary environments. Global and Planetary Change
525 137, 35-53.
526 Šujan, M., Braucher, R., Rybár, S., Maglay, J., Nagy, A., Fordinál, K., Šarinová, K., Sýkora,
527 M., Józsa, Š., Kováč, M., 2018. Revealing the late Pliocene to Middle Pleistocene alluvial
528 archive in the confluence of the Western Carpathian and Eastern Alpine rivers:
529 26Al/10Be burial dating from the Danube Basin (Slovakia). Sedimentary Geology 377,
530 131-146.
531 Šujan, M., Braucher, R., Tibenský, M., Fordinál, K., Rybár, S., Kováč, M., 2020. Effects of
532 spatially variable accommodation rate on channel belt distribution in an alluvial
533 sequence: Authigenic 10Be/9Be-based Bayesian age-depth models applied to the upper
534 Miocene Volkovce Fm. (northern Pannonian Basin System, Slovakia). Sedimentary
535 Geology 397.
536 Šujan, M., Rybár, S., 2014. The development of Pleistocene river terraces in the eastern part of
537 the Danube Basin. Acta Geologica Slovaca 6, 107-122 (in Slovak with English summary).
538 Šujan, M., Rybár, S., Kováč, M., Bielik, M., Majcin, D., Minár, J., Plašienka, D., Nováková,
539 P., Kotulová, J., 2021. The polyphase rifting and inversion of the Danube Basin revised.
540 Global and Planetary Change 196, 103375.
541 Tari, G., 1994. Alpine tectonics of the Pannonian Basin. PhD. Thesis, Rice University, Houston.
542 Tari, G., Arbouille, D., Schléder, Z., Tóth, T., 2020. Inversion tectonics: A brief petroleum
543 industry perspective. Solid Earth 11, 1865-1889.
544 Teodoridis, V., Bruch, A.A., Vassio, E., Martinetto, E., Kvaček, Z., Stuchlik, L., 2017. Plio-
545 Pleistocene floras of the Vildštejn Formation in the Cheb Basin, Czech Republic — A
546 floristic and palaeoenvironmental review. Palaeogeography, Palaeoclimatology,
547 Palaeoecology 467, 166-190.
548 Toonen, W.H.J., Kleinhans, M.G., Cohen, K.M., 2012. Sedimentary architecture of abandoned
549 channel fills. Earth Surface Processes and Landforms 37, 459-472.
550 Vakarcs, G., Vail, P.R., Tari, G., Pogácsás, G., Mattick, R.E., Szabó, A., 1994. Third-order
551 Middle Miocene-Early Pliocene depositional sequences in the prograding delta complex
552 of the Pannonian Basin. Tectonophysics 240, 81-106.

Van Husen, D., 2004. Quaternary glaciations in Austria, Developments in Quaternary Sciences. Elsevier, pp. 1-13.
Van Rijn, L.C., 2020. Erodibility of Mud-Sand Bed Mixtures. Journal of Hydraulic Engineering 146.
van Vliet-Lanoë, B., Magyari, A., Meilliez, F., 2004. Distinguishing between tectonic and periglacial deformations of quaternary continental deposits in Europe. Global and Planetary Change 43, 103-127.
Vandenberghe, J., 2013. Cryoturbation Structures, Encyclopedia of Quaternary Science: Second Edition, pp. 430-435.
Vlačiky, M., Sliva, Ľ., Tóth, C., Karol, M., Zervanová, J., 2008. The fauna and sedimentology of the locality Nová Vieska (Villafranchian, SR). Acta Musei Moraviae, Scientiae geologicae 93, 229-244.
Vlačiky, M., Šujan, M., Rybár, S., Braucher, R., 2017. Nová Vieska locality: fauna, sediments and their dating – new results, 15th predvianočný geologický seminár SGS – Nové poznatky o stavbe a vývoji Západných Karpát, Mente et Maleo, Abstracts, p. 57.
von Blanckenburg, F., 2005. The control mechanisms of erosion and weathering at basin scale from cosmogenic nuclides in river sediment. Earth and Planetary Science Letters 237, 462-479.
Willenbring, J.K., von Blanckenburg, F., 2010. Meteoric cosmogenic Beryllium-10 adsorbed to river sediment and soil: Applications for Earth-surface dynamics. Earth-Science Reviews 98, 105-122.
Wittmann, H., Von Blanckenburg, F., Bouchez, J., Dannhaus, N., Naumann, R., Christl, M., Gaillardet, J., 2012. The dependence of meteoric 10Be concentrations on particle size in Amazon River bed sediment and the extraction of reactive 10Be/ 9Be ratios. Chemical Geology 318-319, 126-138.
Wittmann, H., von Blanckenburg, F., Mohtadi, M., Christl, M., Bernhardt, A., 2017. The competition between coastal trace metal fluxes and oceanic mixing from the 10Be/9Be ratio: Implications for sedimentary records. Geophysical Research Letters 44, 8443-8452.
Yawar, Z., Schieber, J., 2017. On the origin of silt laminae in laminated shales. Sedimentary Geology 360, 22-34.